Photochemistry and Photobiology, 20**, **: *–*

## Special Issue Research Article

# Photoactive Platinum(II) Azopyridine Complexes†

**Sarah J. Farley[1], Luca Salassa[1,2,3,4]*, Ana M. Pizarro[1,5] and Peter J. Sadler[1]***

[1]Department of Chemistry, University of Warwick, Coventry, UK
[2]Donostia International Physics Center, Donostia, Spain
[3]Polimero eta Material Aurreratuak: Fisika, Kimika eta Teknologia, Kimika Fakultatea, Euskal Herriko Unibertsitatea UPV/EHU, Donostia, Spain
[4]Ikerbasque, Basque Foundation for Science, Bilbao, Spain
[5]IMDEA Nanociencia, Madrid, Spain

**Received 13 January 2021, revised 14 February 2021, accepted 18 February 2021, DOI: 10.1111/php.13405**

## ABSTRACT

**Platinum(II) complexes containing the strong π-acceptor *N*,*N*-chelating ligand phenylazopyridine (Ph-azpy) [Pt(*p*-R-Ph-azpy)$X_2$], R = H, $NMe_2$ or OH, X = Cl or $N_3$, have been synthesized and characterized to explore the effects of monodentate ligands and phenyl substituents on their absorption spectra and photoactivation. Time-dependent density functional theory calculations showed that the complexes have a low-lying unoccupied orbital with strong σ-antibonding character toward the majority of the coordination bonds. The UV–visible absorption bands were assigned as mainly ligand-centered or metal-to-ligand charge-transfer transitions, with strong contributions from the chlorido and azido groups. In complexes with substituted Ph-azpy ligands, σ-donation from $NMe_2$ and $OH/O^-$ groups results in a redshift of the main absorption bands compared with unsubstituted Ph-azpy complexes. The diazido complexes are photoactive in solution upon irradiation with either UVA or visible light for R = H or $NMe_2$, or UVA only when R = $OH/O^-$. Intriguingly, the phenolate group of the latter complex undergoes very slow protonation in solution. Biological screening was limited by poor solubility; however, initial tests showed that the phenolato diazido complex is rapidly taken up into the nuclei of HaCaT keratinocytes, which are stained intensely blue, and its cytotoxicity is increased upon irradiation with UVA light.**

## INTRODUCTION

There is current interest in the design of photoactivatable metal complexes for use in phototherapy (1–4). Two such complexes that recently entered clinical use are the Ru(II) complex TLD-1433 and the Pd(II) complex TOOKAD® Soluble. In particular, it is desirable to be able to tune the wavelength of absorption and photoactivation to match the desired penetration depth of the irradiation, ranging from UVA and blue light to the longer depth of penetration of red and near-IR radiation.

Among the most widely used anticancer drugs are Pt(II) complexes, including cisplatin, carboplatin and oxaliplatin. However, there is a need to overcome emerging resistance to these drugs as well as the side effects associated with their use. One potential approach could involve the administration of platinum complexes with low toxicity as inactive prodrugs, which could then be activated specifically in tumors using directed photoirradiation. Octahedral diazido diamine Pt(IV) complexes are promising for such purposes (5–7). Here, we explore the properties of square-planar Pt(II) diazido complexes containing the strong π-acceptor ligand phenylazopyridine, with the aim of generating complexes that absorb strongly in the visible region.

The use of azopyridines as ligands introduces several interesting features into metal complexes. First, they often reduce the reactivity of the coordinated metal. For example, Ru(II) and Os(II) arene, and Ir(III) Cp* anticancer complexes that contain azopyridine ligands can be quite inert toward ligand substitution reactions such as aquation. They are activated in cells by attack of the intracellular thiol glutathione on the azo double bond (8–10). Second, they can introduce intense metal-to-ligand charge transfer (MLCT) and intraligand π–π* transitions into the metal complex, giving rise to strong visible light absorption and intense colors (11). Third, UVA irradiation can induce *trans–cis* isomerization of the N=N bond in monodentate (pyridine *N*-bound) ligands, for example in organo-Pt(II) complexes.

One of the few reports of the use of azopyridine ligands in the design of photoactivatable platinum complexes is that of Chakravarty *et al*. (12). Among the complexes studied was [Pt(Ph-azpy)(an-cat)], where $H_2$an-cat is 4-[2-[(anthracen-9-ylmethylene)amino]ethyl]benzene-1,2-diol, a catechol ligand conjugated to anthracene as a photosensitizer. This complex exhibited a broad charge-transfer band at around 750 nm involving the coordinated catecholate ligand, and photocytoxicity toward HaCaT human skin keratinocytes and MCF-7 breast cancer cells upon irradiation with visible light.

Here, we explore a different approach to controlling the UV–visible absorption of Pt(II) phenylazopyridine complexes by varying the monodentate ligands and the substituents on the

*Corresponding authors email: lsalassa@dipc.org (Luca Salassa), P.J.Sadler@warwick.ac.uk (Peter J. Sadler)
†This article is part of a Special Issue dedicated to the memory of Dr. Karen Brewer.

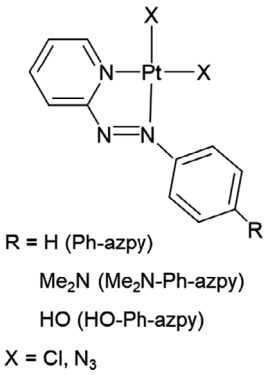


| Complex | Azo ligand | X |
|---|---|---|
| 1 | Ph-azpy | Cl |
| 2 | Ph-azpy | $N_3$ |
| 3 | $Me_2N$-Ph-azpy | Cl |
| 4 | $Me_2N$-Phazpy | $N_3$ |
| 5 | HO-Ph-azpy | Cl |
| 6 | O-Ph-azpy | $N_3$ |

**Figure 1.** Structures of the Pt(II) azopyridine complexes studied in this work.

phenyl ring to prepare six square-planar complexes, [Pt(*p*-R-Ph-azpy)$X_2$], R = H, $NMe_2$ or OH, X = Cl or $N_3$, as illustrated in Fig. 1. We show that both the monodentate ligands and the phenyl substituents can have significant effects on the absorption spectra and photoactivity. We use time-dependent density functional theory (TD-DFT) calculations to assign the transitions and identify the frontier orbitals, and the solution chemistry of the complexes is investigated. Attempts to explore the suitability of these complexes as photoactivatable platinum anticancer prodrugs were limited by their poor solubility in aqueous media, with the exception of the phenolate diazido complex **6**, which showed interesting behavior in aqueous solution and was screened for photocytotoxicity toward immortalized human keratinocytes.

## MATERIALS AND METHODS

*Materials.* 2-(Phenylazo)pyridine (Ph-azpy) and 4-(2-pyridylazo)phenol (HO-Ph-azpy) were kindly donated by Dr Sarah Dougan, and were synthesized as previously described (13). The former was purified by column chromatography prior to use (silica gel, eluting with 100% dichloromethane), whereas the latter was used as received. 4-(2-Pyridylazo)-*N*,*N*-dimethylaniline ($Me_2N$-Ph-azpy) was purchased from Sigma-Aldrich, and *cis*-[Pt$(DMSO)_2Cl_2$] was synthesized as reported (14). UV-grade dioxane (Sigma-Aldrich) and HPLC-grade methanol and water (Fisher) were used as solvents for UV–visible spectroscopy. All other reagents were obtained from commercial sources and were used as received.

*Synthesis of Pt(II) azopyridine complexes. [Pt(Ph-azpy)$Cl_2$] (**1**)*, Ph-azpy (75 mg, 0.41 mmol) was dissolved in dichloromethane (5 mL) and added to a solution of *cis*-[Pt$(DMSO)_2Cl_2$] (174 mg, 0.41 mmol) in dichloromethane (30 mL). After 5 min, the orange solution began to darken and was then stirred at room temperature for 4 h. The solvent volume was reduced, and the mixture stored overnight at 277 K. A brick-red solid was filtered off, washed with dichloromethane and dried under vacuum.

Yield: 165 mg (90%). Elemental analysis: Found: C, 29.36; H, 1.86; N, 9.12. $PtC_{11}H_9N_3Cl_2$ requires: C, 29.41; H, 2.02; N, 9.35%. $^1$H NMR (500 MHz, $CDCl_3$): $\delta$ = 9.89 (d, $^3J(^{195}Pt–^1H)$ 30 Hz, 1H), 8.56 (d, 1H), 8.39 (td, 1H), 7.99 (m, 3H), 7.61 (t, 1H), 7.55 ppm (t, 2H). ESI-MS: 471.97 $[M + Na]^+$, $NaPtC_{11}H_9N_3Cl_2$ requires 471.97 m/z.

*[Pt(Ph-azpy)$(N_3)_2$] (**2**)*, [Pt(Ph-azpy)$Cl_2$] (**1**) (75 mg, 0.17 mmol) was dissolved in dimethylformamide (10 mL), and the mixture was sonicated to ensure dissolution. To this, a solution of $NaN_3$ (109 mg, 1.7 mmol) in methanol (6.5 mL) was added, upon which there was an immediate color change from orange to deep pink. The solution was stirred in the dark at room temperature for 48 h, after which all solvent was removed by rotary evaporation. Water (5 mL) was added to dissolve any excess $NaN_3$, and the insoluble black product was filtered off, washed with small quantities of water, ethanol and diethyl ether, and dried under vacuum.

Yield: 66 mg (85%). Elemental analysis: Found: C, 28.01; H, 1.82; N, 26.50. $PtC_{11}H_9N_9$ requires: C, 28.58; H, 1.96; N, 27.27%. $^1$H NMR (500 MHz, $CDCl_3$): $\delta$ = 9.21 (d, $^3J(^{195}Pt–^1H)$ 27 Hz, 1H), 8.48 (d, 1H), 8.34 (td, 1H), 8.05 (d, 2H), 7.94 (t, 1H), 7.65 (t, 1H), 7.58 ppm (t, 2H). ESI-MS: 485.05 $[M + Na]^+$, $NaPtC_{11}H_9N_9$ requires 485.05 m/z.

*[Pt($Me_2N$-Ph-azpy)$Cl_2$] (**3**)*, $Me_2N$-Ph-azpy (100 mg, 0.44 mmol) was dissolved in dichloromethane (20 mL) and added to a solution of *cis*-[Pt$(DMSO)_2Cl_2$] (185 mg, 0.44 mmol) in dichloromethane (55 mL). Upon mixing, a color change from orange to blue was observed; the solution was then stirred at room temperature for 4 h. The solvent volume was reduced, and the mixture stored overnight at 277 K. A green-gold solid was filtered off, washed with dichloromethane and dried under vacuum. Yield: 195 mg (90%). Elemental analysis: Found: C, 31.62; H, 2.79; N, 11.28. $PtC_{13}H_{14}N_4Cl_2$ requires: C, 31.72; H, 2.87; N, 11.38%. $^1$H NMR (500 MHz, $CDCl_3$): $\delta$ = 9.62 (d, $^3J(^{195}Pt–^1H)$ 30 Hz, 1H), 8.39 (d, 2H), 8.15 (td, 1H), 8.08 (d, 1H), 7.57 (t, 1H), 6.74 (t, 2H), 3.22 ppm (s, 6H). ESI-MS: 498.09 $[M - Cl + MeCN]^+$, $PtC_{15}H_{17}N_5Cl$ requires 497.90 m/z.

*[Pt($Me_2N$-Ph-azpy)$(N_3)_2$] (**4**)*, [Pt($Me_2N$-Ph-azpy)$Cl_2$] (**3**) (25 mg, 0.05 mmol) was dissolved in dimethylformamide (5 mL) to give a blue solution. $NaN_3$ (33 mg, 0.51 mmol) in methanol (2 mL) was added; no color change was observed. The solution was stirred in the dark at room temperature for 48 h; then, water (100 mL) was added and the solution lyophilized. To the residue, water (5 mL) was added to dissolve any excess $NaN_3$, and the insoluble green solid was filtered off, washed with small quantities of water, ethanol and diethyl ether, and dried under vacuum. Yield: 19 mg (75%). Elemental analysis: Found: C, 30.79; H, 2.74; N, 27.42. $PtC_{13}H_{14}N_{10}$ requires: C, 30.89; H, 2.79; N, 27.71%. $^1$H NMR (500 MHz, $CDCl_3$): $\delta$ = 9.01 (d, $^3J(^{195}Pt–^1H)$ 32 Hz, 1H), 8.47 (d, 2H), 8.12 (t, 1H), 8.02 (d, 1H), 7.54 (t, 1H), 6.78 (t, 2H), 3.24 ppm (s, 6H). ESI-MS: 528.09 $[M + Na]^+$, $NaPtC_{13}H_{14}N_{10}$ requires 528.09 m/z.

*[Pt(HO-Ph-azpy)$Cl_2$] (**5**)*, HO-Ph-azpy (56 mg, 0.28 mmol) was dissolved in methanol (50 mL) and added to a solution of *cis*-[Pt$(DMSO)_2Cl_2$] (100 mg, 0.24 mmol) in methanol (100 mL). The mixture was sonicated for five minutes to aid dissolution of the starting materials, during which time it began to darken from orange to a deep red-brown color. It was then stirred overnight at room temperature. The volume was reduced, and the mixture stored at 277 K for 4 h. A brown solid was filtered off, washed with methanol and collected. To ensure total removal of *cis*-[Pt$(DMSO)_2Cl_2$], dichloromethane (8 mL) was added and the mixture stirred, sonicated for 10 s, then filtered off and collected again. Yield: 79 mg (68%). Elemental analysis: Found: C, 27.81; H, 2.15; N, 8.82. $PtC_{11}H_9N_3Cl_2O$ requires: C, 28.40; H, 1.95; N, 9.03%. $^1$H NMR (400 MHz, $d_4$-MeOD): 9.60 (d, $^3J(^{195}Pt–^1H)$ 32 Hz, 1H), 8.59 (d, 1H), 8.48 (td, 1H), 8.03 (d, 2H), 8.00 (t, 1H), 6.91 ppm (t, 2H). ESI-MS: 487.96 $[M + Na]^+$, $NaPtC_{11}H_9N_3Cl_2O$ requires 486.97 m/z.

*Na[Pt(O-Ph-azpy)$(N_3)_2$] (**6**)*, [Pt(HO-Ph-azpy)$Cl_2$] (**5**) (25 mg, 0.05 mmol) was dissolved in dimethylformamide (5 mL) to give a dark orange solution. $NaN_3$ (35 mg, 0.54 mmol) in methanol (2 mL) was added; there was an immediate color change to deep blue. The solution was stirred in the dark at room temperature for 48 h; then, water (100 mL) was added and the solution lyophilized. To the residue, water (5 mL) was added to dissolve any excess $NaN_3$; the product was also partially soluble; however, a quantity of dark blue product was isolated and washed with small quantities of water, ethanol and diethyl ether, and dried under vacuum. Yield: 18 mg (65%). Elemental analysis: Found: C, 26.61; H, 1.79; N, 23.95. $PtC_{11}H_8N_9ONa$ requires: C, 26.41; H, 1.61; N, 25.20%. $^1$H NMR (500 MHz, $CDCl_3$): $\delta$ = 8.63 (d, $^3J(^{195}Pt–^1H)$ 32 Hz, 1H), 8.46 (d, 2H), 8.05 (t, 1H), 7.76 (d, 1H), 7.30 (t, 1H), 6.49 ppm (d, 2H). ESI-MS: 501.04 $[M + H]^+$, $NaPtC_{11}H_9N_9O$ requires 501.04 m/z.

*Note on CHN analyses:* in our experience, the CHN analyses of azido platinum complexes often suffer from problems with combustion, and can give rise to larger deviations from expected values than are normally found for high-purity compounds. For the present compounds, such deviations are apparent for complex **2** (C 0.57%, N 0.77%), complex **5** (C 0.59%) and complex **6** (N 1.25%). However, their other CHN data, and NMR and MS data are consistent with the expected compositions.

*Mass spectrometry.* Electrospray ionization mass spectra were obtained either on a Bruker Esquire2000 Spectrometer or on a Bruker MicroTOF Spectrometer. Samples were prepared either in water or in a methanol/water mixture, and the cone voltage and source temperature varied depending upon the sample. Data were processed using DataAnalysis 3.3 (Bruker Daltonics).

*NMR spectroscopy.* NMR spectra were recorded on Bruker DPX 400 MHz (for $^1$H ), AV 400 MHz or DRX 500 MHz spectrometers. 1D and 2D spectra were recorded using standard Bruker pulse sequences modified by Dr Adam Clarke or Dr Ivan Prokes (University of

Warwick). Unless otherwise stated, spectra were acquired in 5 mm quartz NMR tubes at 298 K. $^1$H chemical shifts ($\delta$, ppm) were referenced to residual protio-solvent resonances: 7.26 ($d_1$-chloroform), 3.31 ($d_4$-methanol) and 2.09 ($d_6$-acetone). Spectral data were processed using either XWIN-NMR (version 2.0 or 3.6, Bruker UK Ltd) or MestReC (version 4.9.9.9, Mestrelab Research, Spain).

*Computational methods.* DFT calculations on the azopyridine ligands and platinum complexes were carried out using Gaussian 03 (15). Geometry optimization of the ground state was performed in the gas phase with the gradient-corrected correlation functional PBE1PBE (16). The LanL2DZ basis set (17) and effective core potential were used for the Pt atom, and the 6–31G** basis set (18) was used for all other atoms. Ligands were optimized at the PBE1PBE/6–31G** level. The nature of all stationary points was confirmed by performing a normal-mode analysis.

Sixteen singlet excited states for the ligands and thirty-two for the complexes were calculated with TD-DFT (19) using ground-state geometries optimized in the gas phase. The conductor-like polarizable continuum model method (CPCM) (20) with methanol as solvent was used to calculate the electronic structures and excited states in solution. The electronic distribution and the localization of the singlet excited states were visualized using the electron density difference maps (EDDMs) (21). GaussSum 1.05 (22) was used for calculation of the EDDMs and for simulation of the electronic spectra.

*Kinetic studies of azopyridine ligands and Pt(II) complexes by UV–visible spectroscopy.* The UV–visible absorption spectra of the ligands Ph-azpy, $Me_2N$-Ph-azpy and HO-Ph-azpy, as well as the complexes **1**–**6**, were monitored over a 12 h period in dioxane at 298 K. Sample preparation, carried out under subdued laboratory light, involved dissolution of the compound in dioxane, filtration, appropriate dilution and, where necessary, addition of acid. To allow for this, a delay of five minutes was set between dissolution and recording the first spectrum. Spectra were subsequently recorded every 2 min for 1 h, every 5 min for a further 1 h, every 10 min for 3 h, then every 30 min for the remaining 7 h. In the case of HO-Ph-azpy and [Pt(HO-Ph-azpy)$Cl_2$] (**5**), 10 μL (~3 equiv.) of 0.01 M $HNO_3$ was added to ensure that the phenolic group remained protonated. For Na[Pt(O-Ph-azpy)$(N_3)_2$] (**6**), the study was carried out in methanol owing to the insolubility of the complex in dioxane.

*Stability of complex **6** in aqueous solution and cell culture medium.* The stability of complex **6** in aqueous solution was monitored at 310 K over a 12 h period by UV–visible spectroscopy. Following dissolution of **6**, spectra were recorded every 2 min for 1 h, every 5 min for a further 1 h, every 10 min for 3 h, then every 15 min for the remaining 7 h. The stability of this complex was also assessed under solution conditions similar to those used in cytotoxicity testing. Following dissolution of the complex in DMSO, appropriate dilutions were performed so that the final solution comprised 1% DMSO, 12.5% saline (0.9% NaCl solution) and 86.5% RPMI-1640 medium. Because the medium is pink in color, a solution of the same composition but without complex was used as a baseline for the UV–visible absorption spectra, so that any absorbance observed was solely from the complex.

*Stability of Pt(II) complexes in acetone.* The stability of complexes **1**–**6** was monitored over time by $^1$H NMR spectroscopy. Saturated solutions of the complexes were prepared in $d_6$-acetone and a spectrum was recorded immediately after dissolution (~5 min); spectra were then re-recorded after 1, 3, 6, 18 and 113 days. Samples were stored at ambient temperature in the dark between measurements.

*Photoreactions.* Photoreactions of complexes **1**–**5** in dioxane, and complex **6** in methanol, were monitored by UV–visible spectroscopy. For all complexes, irradiations were performed using an LZC-ICH2 photoreactor equipped with LZC-UVA lamps ($\lambda_{max}$ = 365 nm, $P$ (power level) = 1.7–2.2 mW cm$^{-2}$) and LZC-VIS UV–visible light lamps ($\lambda_{max}$ = 400–700 nm, $P$ = 0.27–0.29 mW cm$^{-2}$). For complexes **1** and **2**, irradiations in the visible region were also carried out using four green LEDs ($\lambda_{max}$ = 525 nm, $P$ = 0.19 mW cm$^{-2}$). For complex **3**, nonirradiated controls were included, as the spectral profile of this complex changed over time in the dark. These controls were placed in the photoreactor but were covered in aluminum foil to avoid exposure to light.

All irradiations were carried out at 298 K unless otherwise stated, with spectra recorded after the following total irradiation times: 0.5, 1, 2, 3, 5, 10, 15, 20, 30, 45, 60, 90 and 120 min.

*Fluorescence spectroscopy.* Fluorescence spectra of the ligands Ph-azpy, $Me_2N$-Ph-azpy and HO-Ph-azpy, and of complexes **1**–**6**, were recorded at 298 K in dioxane. $\lambda_{ex}$ was set to the $\lambda_{max}$ for each absorption band of the compound.

*Cytotoxicity testing.* Experiments to determine the cytotoxicity of **6** toward the human ovarian A2780 cancer cell line were performed according to a previously published protocol (23). The A2780 human ovarian cancer cell line was obtained from the ECACC (European Collection of Cell Culture, Salisbury, UK). Cells were grown in RPMI 1640 medium with 1% 2 mM L-glutamine supplemented with 10% fetal calf serum and 1% penicillin/streptomycin and were maintained under standard tissue culture conditions of 310 K and 5% $CO_2$.

After plating, human ovarian A2780 cancer cells were allowed to grow for 48 h before addition of the complexes at concentrations ranging from 5 to 200 μM. Solutions of the complexes were prepared in 0.5% DMSO (v/v) to assist dissolution. Each concentration was added in triplicate, and the experiment was carried out three times. Cells were exposed to the complexes for 24 h, washed with PBS, supplied with fresh medium and allowed to grow for three doubling times (72 h), and then the protein content was measured (proportional to cell survival) using the sulforhodamine B (SRB) assay (24). Cisplatin was used as a positive control (half-maximum inhibitory concentration ($IC_{50}$) = 1.3 ± 0.1 μM).

*Photocytotoxicity testing.* The photocytotoxicity of complex **6** toward the HaCaT keratinocyte human skin cell line was determined by Dr Julie Woods and Kim Robinson in a specially adapted photobiology laboratory, with ambient light levels below 1 lux (Solatell), at the Photobiology Unit in Ninewells Hospital, Dundee, UK. HaCaT cells were maintained in Dulbecco's modified Earle's medium containing 5% fetal bovine serum. Complexes were dissolved in Earle's balanced salt solution before being applied to cells. Cells were seeded at a density of around 70 000 cells per cm$^2$ and left to adhere overnight. After washing cells with PBS, the test compound was added in Earle's solution and incubated for 1 h (310 K/5% $CO_2$). After this time, cells were irradiated by a bank of 2 ft × 6 ft Cosmolux RA Plus (Cosmedico) 15 500/100 W UVA light sources (5 J cm$^{-2}$, $\lambda_{max}$ = 365 nm), each filtered to attenuate UVB and UVC wavelengths. The total irradiation time was 50 min, to give a dose equivalent to around 15–60 min sunlight received on a typical UK midday, and reflects the clinical conditions used for light-activated drugs. After irradiation, the solution was removed and the cells were thoroughly washed and returned to the incubator in complete growth medium. Photocytotoxicity was determined 24 h later using the neutral red uptake assay (25,26), a test designed to compare the toxicity of a drug plus light with that of the drug alone. The amount of test compound required to inhibit dye uptake by 50% (the $IC_{50}$ value) was determined by nonlinear regression (GraphPad Prism). Goodness of fit was determined by the 95% confidence intervals and the $R^2$ value. Concentrations were added in triplicate, and each experiment was repeated three times, using chlorpromazine as a positive control ($IC_{50}$ (CPZ + UVA) = 3.6 μM).

## RESULTS AND DISCUSSION

### Synthesis and reactivity of Pt(II) complexes

Six Pt(II) dichlorido and diazido complexes containing three azopyridine ligands [Pt(*p*-R-Ph-azpy)$X_2$], R = H, $NMe_2$ or OH, X = Cl (complexes **1**, **3** and **5**, respectively) or $N_3$ (complexes **2**, **4** and **6**, respectively) were synthesized and characterized (Fig. 1). Pt(II) chlorido complexes of several azopyridine derivatives have been reported in the literature (27,28). Using *cis*-[Pt$(DMSO)_2Cl_2$] instead of $[PtCl_4]^{2-}$ as the starting material gave analytically pure complexes **1** and **3** in higher yields (65–90%) and on a shorter timescale, owing to the ease of replacement of the two DMSO groups by incoming ligands (29). The yield was reduced, however, in the synthesis of **5** owing to the need for an additional purification step.

Formation of a Pt(II) azido complex is commonly carried out by chloride extraction with silver nitrate in aqueous solution, followed by the addition of sodium azide (30). However, the poor aqueous solubility of the Pt(II) chlorido complexes, combined

**Table 1.** Selected bond distances (Å) of complexes **1**–**6** in the calculated ground-state geometries, and comparison with the X-ray crystal structure of **1**.

| Pt(II) chlorido complex | N=N | Pt–N(py) | Pt–N(aza) | Pt–Cl (*trans*-py) | Pt–Cl (*trans*-aza) |
|---|---|---|---|---|---|
| [Pt(Ph-azpy)$Cl_2$] (**1**) *Calculated* | 1.275 | 2.016 | 2.003 | 2.316 | 2.318 |
| [Pt(Ph-azpy)$Cl_2$] (**1**) *X-ray* | 1.291(9) | 2.018(8) | 1.965(8) | 2.281(2) | 2.288(3) |
| [Pt($Me_2$N-Ph-azpy)$Cl_2$] (**3**) | 1.286 | 2.012 | 2.019 | 2.326 | 2.324 |
| [Pt(HO-Ph-azpy)$Cl_2$] (**5**) | 1.282 | 2.013 | 2.002 | 2.325 | 2.325 |
| **Pt(II) azido complex** | **N=N** | **Pt–N(py)** | **Pt–N(aza)** | **Pt–$N_3$ (*trans*-py)** | **Pt–$N_3$ (*trans*-aza)** |
| [Pt(Ph-azpy)$(N_3)_2$] (**2**) | 1.280 | 2.021 | 2.019 | 2.002 | 1.989 |
| [Pt($Me_2$N-Ph-azpy)$(N_3)_2$] (**4**) | 1.289 | 2.017 | 2.049 | 2.012 | 1.995 |
| Na[Pt(O-Ph-azpy)$(N_3)_2$] (**6**) | 1.327 | 2.013 | 2.080 | 2.039 | 2.018 |

with the reported unsuitability of this method for Pt(II) bipyridine complexes (31), led to the use of an alternative method in this case, whereby sodium azide was added directly to the complex in DMF. This approach, previously used in the synthesis of Pt(II) azido complexes containing bipyridines (32), was found to be equally suitable in this case, and the required complexes were isolated in good yields.

Complex **6** was isolated as a salt in which the azopyridine ligand was present in its deprotonated phenolate form, Na[Pt(O-Ph-azpy)$(N_3)_2$]. Subsequent experiments indicated that the phenolic OH group has a p$K_a$ of approximately 5.7 when the ligand is coordinated to Pt(II) and that the methanolic solution of sodium azide used in the reaction was sufficiently basic to effect deprotonation. The presence of excess sodium azide meant that it was not possible to isolate the protonated product by acidifying the reaction solution during synthesis, as this would produce hydrogen azide, an extremely toxic gas. Further attempts to isolate the protonated product by acidification of an aqueous solution of the isolated deprotonated sample were also unsuccessful. Several metal complexes of HO-Ph-azpy have previously been found to be unstable and sensitive to changes in pH (33).

The square-planar structure of [Pt(Ph-azpy)$Cl_2$] (**1**) was confirmed by single-crystal X-ray diffraction, and corresponded well with that previously reported (27).

We next attempted to oxidize [Pt(Ph-azpy)$(N_3)_2$] (**2**) to the Pt(IV) *trans*-dihydroxido complex, because oxidation of Pt(II) azido complexes has previously been found to result in strong azide-to-Pt(IV) charge-transfer bands (6). However, reactions with hydrogen peroxide in aqueous solution or in acetone (34) and use of the organic oxidizing agent *meta*-chloroperoxybenzoic acid were all unsuccessful, the latter appearing to decompose the azopyridine ligand. The oxidation of [Pt(bipyridine)$(N_3)_2$] and similar complexes is reported to be difficult to achieve, due to the π-acceptor nature of bipyridine and its ability to stabilize metals in their lower oxidation states (35). Ph-azpy is a stronger π-acceptor than is bipyridine, as demonstrated by the greater stability of [Ru(Ph-azpy)$_2Cl_2$] compared with [Ru(bipyridine)$_2Cl_2$] with respect to oxidation to Ru(III) (36). Therefore, it is perhaps not surprising that the oxidation of **2** is not facile.

### Computed geometries of Pt(II) complexes

DFT calculations showed that, upon coordination to Pt(II), the phenyl ring of the azopyridine ligand is twisted out of the Pt–pyridine–azo plane by between 29° and 39° in complexes **1**–**5**. In complex **6**, however, this twist is reduced to 3° and the ligand remains essentially planar. Selected calculated bond lengths for complexes **1**–**6** are reported in Table 1. In the case of complex **1**, they compare well with those from the crystal structure. In all of the chlorido complexes (**1**, **3** and **5**), the N=N bond (1.28–1.29 Å) of the azopyridine ligand lengthens to a similar extent upon coordination. The Pt–Cl bonds are of a similar length (around 2.32 Å) in all complexes, despite differing ligands in the *trans* position (pyridyl and aza nitrogens). In the azido complexes, the N=N distances are similar to those in the chlorido

**Table 2.** Wavelength of maximum absorbances and extinction coefficients for azopyridine ligands and complexes **1**–**6** in methanol and dioxane.

| | Methanol | | Dioxane | |
|---|---|---|---|---|
| Compound | $\lambda_{max}$ (nm) | ε ($M^{-1}$ $cm^{-1}$) | $\lambda_{max}$ (nm) | ε ($M^{-1}$ $cm^{-1}$) |
| Ph-azpy | 222 | 9000 | 222 | 11 200 |
| | 317 | 14 100 | 315 | 16 400 |
| | 441 | 500 | 452 | 300 |
| $Me_2$N-Ph-azpy | 273 | 8700 | 258 | 9100 |
| | 432 | 29 000 | 418 | 44 300 |
| HO-Ph-azpy† | 247 | 8700 | 248 | 9300 |
| | 357 | 21 600 | 355 | 22 100 |
| **1** | 267 | 7500 | 222 | 11 200 |
| | 381 | 13 500 | 395 | 16 400 |
| | 495 | 3200 | 452 | 3000 |
| **2** | 380 | 8700 | 391 | 9100 |
| | 529 | 3700 | 566 | 4300 |
| **3**‡ | 298 | 4400 | 301 | 7200 |
| | 602 | 16 000 | 613 | 19 600 |
| | | | 647 | 22 000 |
| **4**‡ | 293 | 7700 | 298 | 9800 |
| | 614 | 24 000 | 618 | 28 600 |
| **5**† | 272 | 11 000 | 273 | 12 200 |
| | 475 | 17 000 | 461 | 18 900 |
| | | | 481 | 19 800 |
| **6** | 270 | 7900 | n.d. | n.d. |
| | 340 | 4000 | | |
| | 584 | 22 900 | | |
| | 619 | 25 900 | | |

n.d., not determined. †Acidified with 3 equiv. $HNO_3$. ‡95:5 methanol/dioxane:DMF.

analogs, with the exception of complex **6** in which this bond is approximately 0.04 Å longer.

### UV–visible absorption spectra of azopyridine ligands and Pt(II) complexes

UV–visible absorption spectra of the three azopyridine ligands and complexes **1**–**6** were recorded in both methanol and dioxane (Table 2).

TD-DFT calculations were used to assign the absorption bands of the spectra in methanol. Figure 2 shows these overlaid with the experimental spectra for complexes **2** and **5**, and includes the EDDMs of the lowest-energy singlet transition in each case. TD-DFT results for the other complexes and ligands are in the Supporting Information (Tables S1 and S2, Figures S1 and S2).

The main absorption band of Ph-azpy in methanol is centered at 317 nm, corresponding to a π–π* transition in which electron density migrates onto the aza nitrogens. A weak band is also seen at 441 nm in the experimental spectrum, resulting from a formally forbidden n–π* transition. $Me_2N$-Ph-azpy displays a strong absorption band at 432 nm, arising from a mixed π–π*/CT state in which charge transfer from the $NMe_2$ group makes a strong contribution. This results in the redshift of this band compared with the purely π–π* transition of Ph-azpy. Consistent with the σ-donating ability of the *para* substituent on the phenyl ring (H < OH < $NMe_2$), a significant charge-transfer contribution is also seen in the main transition of HO-Ph-azpy, although to a lesser extent than in $Me_2N$-Ph-azpy. Higher-energy absorptions in both $Me_2N$-Ph-azpy and HO-Ph-azpy can be ascribed to π–π* states. Comparing the spectra of these ligands in dioxane and methanol, the transitions display solvatochromism, as expected from their assigned character. Although dioxane is known to show anomalous solvatochromic effects (37), in this case the expected trends are observed. The π–π* bands are redshifted in the more polar methanol, because attractive polarization forces between the solvent and the absorbing molecule lower the energy of the excited state to a greater extent than they do the ground state, decreasing the energy between the two. By contrast, the n–π* transition of Ph-azpy is blueshifted in methanol; this is due to the increased solvation of the lone pair in a more polar solvent, decreasing the energy of the n orbital (38).

The spectrum of **1** consists of a main band centered at 381 nm, with a weaker band at lower energy. The three transitions that comprise the main band all have mixed character, with electron density migrating to the azo group and the pyridyl ring. The formally forbidden n–π* band at lower energy is more intense here than in the case of Ph-azpy. Complex **2** shows a different spectral profile. The band centered at 380 nm results from a primarily ligand-centered transition with some contribution from the metal, whereas a lower-energy band at 529 nm arises from an MLCT transition with a very strong contribution from the azido ligands.

The main absorption band of **3** arises from a ligand-centered transition in which electron density migrates from the $NMe_2$ region to the aza nitrogens, with only a small involvement of the

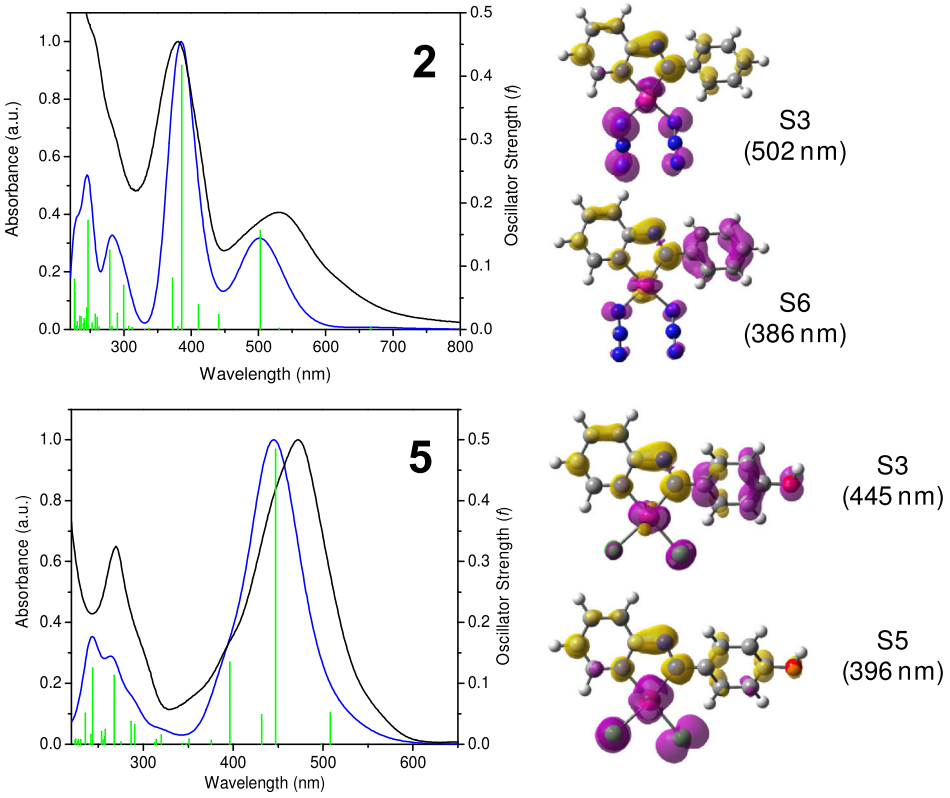


**Figure 2.** Left, normalized absorption spectra for azido complex **2** and chlorido complex **5** in methanol (black) and their corresponding TD-DFT spectra (blue). Calculated singlet electronic transitions are shown as green vertical bars with heights equal to their oscillator strength. Right, EDDMs of selected low-energy singlet electronic transitions for each complex. Electron density migrates from magenta to yellow areas.

metal and chlorido ligands. A lesser contribution to this absorption band is made from a transition at slightly higher energy, which is MLCT in character with a strong involvement of the chlorido ligands. The spectrum of **4** is similar, with an asymmetric band centered at 614 nm, again comprising two transitions. Although charge transfer (from the $NMe_2$ group to the azo nitrogens and the pyridyl ring) dominates the main transition, the metal and azido groups also contribute. The second transition is MLCT in character, with a strong contribution from the azido groups. The relatively broad absorption band in the spectrum of **5** results from two main transitions, with two others making a lesser contribution. The dominant transition is mixed in character, in which electron density migrates to the azo group and pyridyl ring; this is similar to that seen for **1** but in this case there is also contribution from the OH group. The second transition is MLCT in character, with strong involvement of the chlorido groups. Complex **6** shows the poorest agreement between theoretical and experimental spectra; however, the nature of the transitions involved can still be established. It has been observed previously that such predictions are less valid in the presence of strongly electron-donating or electron-withdrawing groups (35); it is assumed that the calculated energy of the orbitals is less accurate in these cases. Three main transitions comprise the absorption band. All are MLCT in character and have strong contributions from the azido ligands, with charge transfer from the oxygen involved to various extents.

The influence of the $NMe_2$ and OH groups of complexes **3**–**6** can be seen by the redshift and the increased molar extinction coefficient of the absorption bands compared with complexes **1** and **2**. σ-Donation from these groups decreases the π-accepting capability of the azo group, increasing the energy of the metal-based orbitals and therefore decreasing the energy of the MLCT transitions. A similar decrease in energy is seen for ligand-centered transitions, owing to the increased delocalization of electron density.

### Effect of pH on the absorption spectra of complexes 3 and 5

The effect of charge transfer from the $NMe_2$ and OH groups on the absorption properties of these complexes is demonstrated by the UV–visible absorption spectra of complexes **3** and **5** at varying pH values (Fig. 3). At very low pH (around 0), the $NMe_2$ group of **3** is protonated and essentially all donating ability is lost; the solution turns from deep blue to orange and the spectral profile resembles that of [Pt(Ph-azpy)$Cl_2$] (**1**). The p$K_a$ value of complex **3** is lower than that of the free ligand (2.11 (11)), reflecting the greater conjugation of the nitrogen lone pair into the π system when the ligand is coordinated to Pt(II). Similarly, the σ-donating ability of the OH group of complex **5** is greatly enhanced upon deprotonation, as can be seen by the large redshift in the main absorption band. The p$K_a$ of the OH group of this complex is around 5.7, significantly lower than that of the free ligand (8.08). A similar effect was observed for the Ru(II) complex [($\eta^6$-*p*-cymene)Ru(HO-Ph-azpy)Cl]$PF_6$, for which the p$K_a$ decreased to 6.48 upon coordination, and for Ir(III) Cp* complexes, for which the p$K_a$ values range from 3.9 to 6.5 (10). This suggests that electron density from the phenolate group is more readily delocalized in the metal complex. Additionally, at physiological pH (around 7.4), the complex will exist predominately in its deprotonated form, with an overall negative charge.

### Fluorescence studies of Pt(II) complexes

The three azopyridine ligands and complexes **1**–**6** were found to be nonemissive under the conditions used (298 K, dioxane).

### Stability of Pt(II) complexes in solution and cell culture media

The NMR spectra of complexes **1**–**6**, recorded in acetone, showed no change over a period of 113 days after storage at ambient temperature in the dark. It can therefore be concluded that these complexes are relatively stable under these conditions. Conversely, the Au(III) complex [Au(Ph-azpy)$Cl_2$]Cl is reported to undergo a metal-mediated reaction to form a cationic, tricyclic organic derivative of Ph-azpy over 12 days in an acetone solution. This cation showed higher cytotoxicity than the parent complex in a number of cancer cell lines (39). Although Pt(II) is isoelectronic and often isostructural with Au(III) (square-planar $5d^8$), the two display markedly different chemistries, with Au(III) being a stronger oxidant.

The absorption spectrum of Na[Pt(O-Ph-azpy)($N_3$)$_2$] (**6**) was also followed over a 12-hour period in unbuffered aqueous solution (Fig. 4). The main absorption bands at around 600 nm decreased rapidly over time, with the absorbance at 594 nm decreasing by 16% in the six minutes after the first acquisition, followed by the emergence of a new peak at 425 nm. The change was also noted visually, as the intense blue color had been lost by the end of the experiment and the solution appeared pale gray-brown. Comparing the final spectrum with those

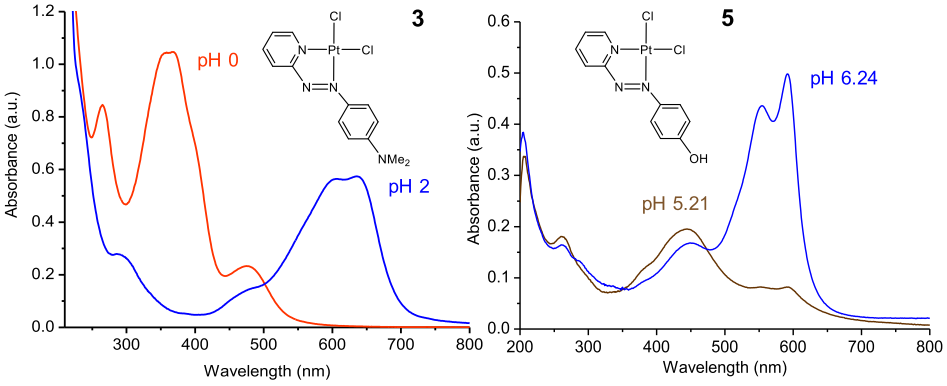


**Figure 3.** The absorption spectra of complexes **3** and **5** at different pH values.

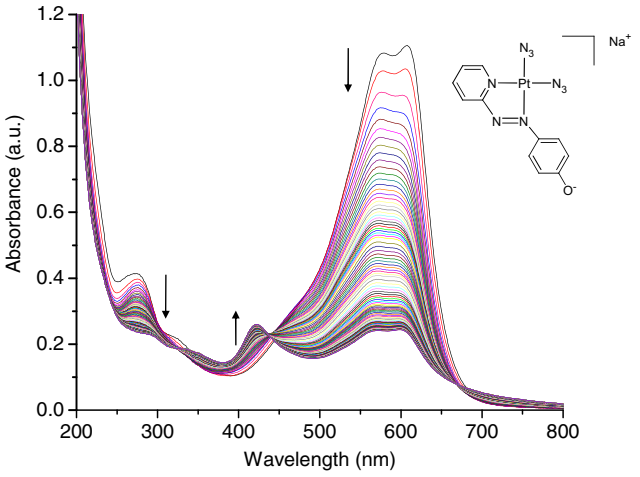


**Figure 4.** The change in absorption profile of **6** over a 12 h period in unbuffered aqueous solution, indicative of the slow protonation of the phenolate oxygen, perhaps coupled to another structural change.

obtained during the pH titration experiment, it appears that the phenolate group of **6** became protonated over time in water. This was confirmed by the addition of 2 molar equivalents of $HNO_3$, after which the peak at 425 nm continued to grow and the two peaks at around 600 nm further decreased in intensity. Conversely, the addition of dilute NaOH restored the spectrum to its original profile.

Importantly, the observed rate of change is much slower than expected, because protonation is typically instantaneous. This reduced rate might indicate the involvement of the phenolate group in intermolecular interactions, reducing its tendency to protonate. Indeed, in the X-ray structures of cyclopentadienyl Ir(III) HO/O-phenylazopyridine complexes, the phenol and phenolate oxygens are involved in strong hydrogen bonds either with a neighboring Ir(III) complex or to solvent (MeOH) (10). The high stability of complex **6** in methanol also supports this possibility. The possibility that protonation is coupled to another slower process, such as ring-opening, is also worthy of further investigation.

The stability of complex **6** in buffered (pH 7.3) RPMI cell culture medium was investigated to mimic the conditions used for cytotoxicity and phototoxicity testing. A similar but much reduced change was seen in this case (Figure S3), indicating that the complex remained predominantly in its deprotonated form during these experiments. This is supported by observations during the cell tests, in which the blue color of the solution remained following the 24-hour exposure of the cells to the drug.

### Photoreactions of Pt(II) complexes

The photoreactions of the Pt(II) complexes **1–6** upon irradiation with UVA and visible light were followed by UV–visible absorption spectroscopy. Experiments were carried out in dioxane owing to the increased solubility in this solvent over methanol, with the exception of complex **6**, for which methanol was used. Unless otherwise stated, the power levels and total irradiation times were as described in the section entitled "Photoreactions."

The spectral profile of **1** remained essentially unchanged after 120 min irradiation with UVA. The main absorption band at 395 nm showed only a small decrease of 2%. This decrease continued upon prolonged irradiation, to a total of 4% after 210 min. Similarly, no change was seen after 120 min irradiation with white light or with green light.

Irradiation with UVA resulted in a decrease in intensity of both main bands in the absorption spectrum of the diazido complex **2** (Fig. 5A). The lower-energy band (566 nm) showed the most rapid change in absorbance, decreasing to less than half of its initial value after 45 min. Upon further irradiation a slight increase in intensity was seen, similar to the remainder of the lower-energy region of the spectrum in which the absorbance increased gradually throughout the experiment. The band at 391 nm also decreased in intensity upon irradiation throughout the experiment. After 45 min, a new peak became apparent at 325 nm, which increased in intensity upon further irradiation. By the end of the experiment, the sample had decolorized significantly, from deep pink to pale brown.

Irradiation with white light also led to a decrease in intensity of both main bands in the spectrum of **2**. Similar changes in the spectral profiles suggest that the same reaction is occurring upon irradiation with both UVA and visible light. However, in the case of visible light the rate of change was slower. After 120 min of irradiation, the band at 566 nm was still decreasing in intensity and the new peak at 325 nm had not clearly resolved. No change was seen in the spectral profile of **2** after 120 min of irradiation with green light (Figure S4).

Attempts to identify the photoproducts of these reactions were unsuccessful. No platinum-containing species could be detected by mass spectrometry, and the poor solubility of the complex in many solvents suitable for irradiation experiments limited attempts to follow the reactions by NMR. The spectrum of the initial complex in dioxane solution showed only weak signals, the intensities of which were rapidly lost upon irradiation. Further work is warranted to investigate the possible production of singlet oxygen and radicals.

Complexes **3** and **5** can be regarded as essentially stable under the different irradiation regimes; after 120 min irradiation, no significant changes were observed in the main absorption bands of these complexes.

The irradiation of complex **2** with UVA light resulted in changes to the main absorption band at 618 nm. Initially, this band decreased in intensity with a broadening of the maxima, and after 30 min, it began to resolve into two separate peaks. Upon further irradiation, the peak at lower energy (621 nm) decreased in intensity faster than that at higher energy (574 nm). Irradiation was continued beyond 120 min, with additional spectra recorded at 180 and 240 min. The trend continued, although the intensity difference between the two peaks began to decrease. A decrease in the higher-energy absorption band at 298 nm was also observed. Irradiation with white light induced similar spectral changes to those seen upon irradiation with UVA, although at a slower rate. In comparison with complexes **2** and **4**, relatively little change was seen in the absorption spectra of azido complex **6** upon irradiation (Fig. 5).

Attempts were made to rationalize the observed behavior considering information from the TD-DFT calculations, which predicted the nature of the transitions and the orbitals involved in singlet excited states. Complexes **1–6** all contain an orbital with σ-antibonding character toward most of the molecule (Figure S5): LUMO + 1 for all except complex **2** (LUMO + 2). The strong antibonding character suggests that all transitions that

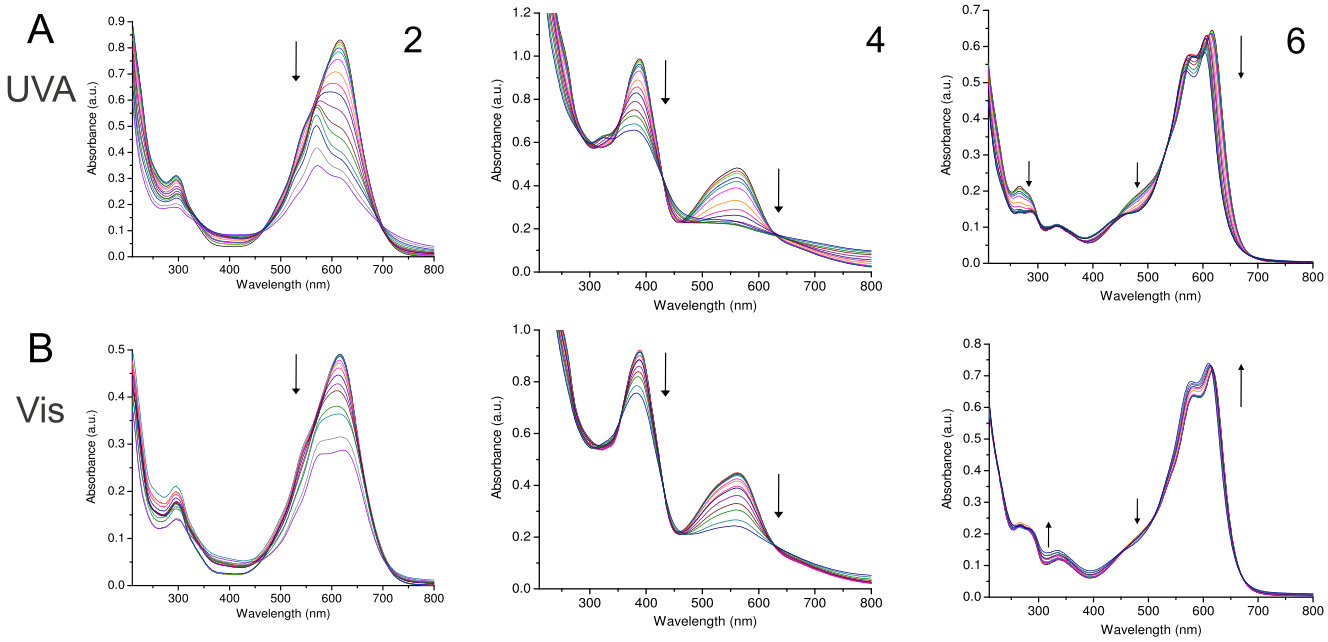


**Figure 5.** UV–visible absorption spectra of diazido complexes **2, 4** and **6** after irradiation with (A) UVA and (B) visible white light, over 120 min in dioxane.

have contributions from this orbital could lead to ligand dissociation or merely to a lengthening of the appropriate bonds (40). This could explain why none of the chlorido complexes seem to be photoactive, despite having accessible transitions (albeit with low probabilities) that involve the population of an antibonding orbital. In the case of the azido complexes, dissociation may be more probable. The azido group is known to display a rich photochemistry, involving the generation of nitrenes and azidyl radicals among other species (41,42), both of which could induce further reaction or decomposition of the photoproducts.

Complex **2** is the most photoactive of the three azido complexes. The strongest predicted transition in this complex (386 nm, with an oscillator strength $f$ of 0.42) has a small (9%) contribution from a HOMO → LUMO + 2 transition, corresponding to population of this strongly antibonding orbital. An additional transition at 372 nm has a much smaller oscillator strength ($f = 0.08$) but a large contribution from the HOMO → LUMO + 2 transition (59%), and is also likely to be significant.

The changes in spectral profile of **2** are similar upon irradiation with UVA or visible light, although occur at a slower rate in the case of the latter. The transitions around 386 nm and 372 nm could potentially be accessed by the visible light source used, as its output spectrum shows spikes of intensity in this region. The energy of the green LEDs ($\lambda_{max} = 525$ nm) was insufficient to induce dissociative transitions and resulted in no change to the absorption spectrum of **2**. Because LUMO + 2 is σ-antibonding toward most of the bonds in the molecule, it is likely that dissociation of the complex is extensive. The loss of the intense color and the rapid decrease in signal intensity in both the absorption and the NMR spectra are consistent with significant decomposition. However, elucidation of the photoproducts may be difficult even if dissociation is less extensive. For example, were free azopyridine to be released it would undergo *cis–trans* isomerization upon irradiation, resulting in changes to the spectral profile that would hinder its identification. According to computational data, similar considerations can be made for complexes **4** and **6**.

### Cytotoxicity and photocytotoxicity of complex 6

The cytotoxicity of several Ru(II) complexes of azopyridines has been reported (11), as well as that of an Au(III) Ph-azpy complex (39). Reports on the cytotoxicity of Pt(II) azopyridine complexes are scarce; however, Chakravarty *et al.* (12) found that [Pt(Ph-azpy)(an-cat)] showed remarkable light-induced cytotoxicity in HaCaT and MCF-7 cells, with $IC_{50}$ values 10-fold lower after irradiation with visible light (400–700 nm) than in the dark. It was suggested that the photoinduced cytotoxicity of these complexes could be associated with reduction of the coordinated azo bond of Ph-azpy by intracellular glutathione, triggering the release of the catecholate ligand.

The lack of aqueous solubility of the complexes synthesized here limited cell testing of all but complex **6**, which is reasonably water soluble due to its isolation as a sodium salt. Complex **6** was tested against the A2780 human ovarian cancer cell line, showing moderate cytotoxicity with an $IC_{50}$ value of 67.7 ± 8.9 μM upon exposure to the cells for 24 h. It is noteworthy that, although the complex remains predominately deprotonated in cell culture media, it may become protonated upon uptake into certain organelles—such as lysosomes—in which the pH is lower.

Encouraged by the cytotoxicity and photoactivity data, complex **6** was tested for photocytotoxicity toward immortalized HaCaT keratinocytes. The experiments were carried out as described in the section "Photocytotoxicity testing", that is, incubation of the cells with the complex for 1 h, followed by 50 min of UVA irradiation. The cytotoxic effect exerted by this complex was stronger upon irradiation with UVA light ($IC_{50} = 72.1$ μM) than in the dark (sham-irradiated control; $IC_{50} = 112.9$ μM),

indicating a 36% increase in the cytotoxicity of **6** upon UVA irradiation.

During testing, it was observed that the intense blue color of the complex caused staining of the cells, and thus provided a means of visualizing the complex within the cells. This staining was evident in the majority of cells in the sample, estimated at around 80% by visual inspection (data not shown). Following the 1 h incubation period prior to irradiation, the blue color appeared to be localized in the nuclear region, with only punctate staining of the cytoplasm (Figure S6). This suggests that the platinum complex reaches the nucleus, because the ligand alone does not give rise to a blue solution, and that uptake into the nucleus is rapid.

Several observations during the testing of this complex warrant further investigation. The punctate staining in the cytoplasm could result from accumulation in mitochondria as well as in the nucleus, indicating a possible targeting of cellular DNA.

## CONCLUSIONS

UV–visible absorption spectra of Pt(II) chlorido complexes of azopyridine ligands showed very little change upon irradiation with UVA and visible light. However, the Pt(II) azido complexes **2** and **4** were found to be photoactive in both cases, with dissociation likely induced by population of a σ-antibonding orbital. Although complex **2** showed similar changes upon irradiation with both UVA and visible light, complex **4** showed differing behavior between the two; it is likely that different transitions were induced in each case, giving rise to different photoproducts. Complex **6** showed some photoactivity upon irradiation with UVA light, but very little was observed with visible light. This complex showed moderate cytotoxicity against the human ovarian A2780 cancer cell line ($IC_{50}$ = 67.7 μM). It was also cytotoxic toward HaCaT keratinocytes, and its activity increased upon irradiation with UVA light, with $IC_{50}$ values of 112.9 μM in the dark and 72.1 μM after irradiation. This complex was found to stain treated cells blue, enabling its location within the cells to be visualized without labeling.

One aim of this work was to synthesize Pt(II) azido complexes with ligands that exhibit strong absorbance in the visible region, to investigate whether this would lead to photoactivity upon irradiation at these wavelengths. As well as strong absorbance in the visible region, these complexes have a large scope for design by, for example, changing the substituents on the phenyl ring, which has been shown here to have a considerable influence on their properties. These results therefore suggest that further exploration of the use of ligands that absorb strongly in the visible region may lead to successful attempts to increase the wavelength of photoactivation of platinum azido complexes.

*ACKNOWLEDGEMENTS*—We thank the MRC (grant number G0701062), EPSRC (grant numbers EP/G006792 and EP/F034210/1) and EU FP7 (grant number 20377; MC fellowship for LS). LS acknowledges the Severo Ochoa Centres of Excellence Program of the Spanish State Research Agency (grant number CEX2018-000867-S; DIPC) for funding and the Spanish Multi-MetDrugs network (RED2018-102471-T) for fruitful discussion. AMP acknowledges funding from the MINECO of Spain (SEV-2016-0686 and CTQ2017-84932-P). We also thank Dr Julie Woods and Kim Robinson (University of Dundee) for phototoxicity testing, and Dr Lijiang Song and Dr Ivan Prokes (University of Warwick) for help with MS and NMR, respectively.

## SUPPORTING INFORMATION

Additional supporting information may be found online in the Supporting Information section at the end of the article:

**Figure S1**. Normalized absorption spectra of azopyridine ligands in methanol and their corresponding TD-DFT spectra, and EDDMs of selected low-energy singlet electronic transitions for each ligand.

**Table S2**. Calculated singlet electronic transitions for complexes **1**–**6** in methanol.

**Figure S2**. Normalized absorption spectra for complexes **1**, **3**, **4** and **6** in methanol and their corresponding TD-DFT spectra.

**Figure S3**. The change in absorption profile of complex **6** over a 12 h period in cell culture medium.

**Figure S4**. UV–visible absorption spectra of complex **2** following irradiation with green light over 120 min in dioxane.

**Figure S5**. Selected orbitals of Pt(II) azopyridine complexes.

**Figure S6**. A microscope image of HaCaT cells prior to irradiation, 1 h after addition of complex **6**.

**Table S1**. Calculated singlet electronic transitions for azopyridine ligands in methanol.

## REFERENCES

1. McFarland, S. A., A. Mandel, R. Dumoulin-White and G. Gasser (2020) Metal-based photosensitizers for photodynamic therapy: The future of multimodal oncology? *Curr. Opin. Chem. Biol.* **56**, 23–27.
2. Monro, S., K. L. Colón, H. Yin, J. Roque III, P. Konda, S. Gujar, R. P. Thummel, L. Lilge, C. G. Cameron and S. A. McFarland (2019) Transition metal complexes and photodynamic therapy from a tumor-centered approach: Challenges, opportunities, and highlights from the development of TLD1433. *Chem. Rev.* **119**, 797–828.
3. Imberti, C., P. Zhang, H. Huang and P. J. Sadler (2020) New designs for phototherapeutic transition metal complexes. *Angew. Chem. Int. Ed.* **59**, 61–73.
4. Shi, H. and P. J. Sadler (2020) How promising is phototherapy for cancer? *Br. J. Cancer* **123**, 871–873.
5. Bednarski, P. J., F. S. Mackay and P. J. Sadler (2007) Photoactivatable platinum complexes. *Anticancer Agents Med. Chem.* **7**, 75–93.
6. Venkatesh, V. and P. J. Sadler (2018) Platinum(IV) prodrugs. *Met. Ions Life Sci.* **18**, 69–107.
7. Shi, H., C. Imberti and P. J. Sadler (2019) Diazido platinum(IV) complexes for photoactivated anticancer chemotherapy. *Inorg. Chem. Front.* **6**, 1623–1638.
8. Needham, R. J., C. Sanchez-Cano, X. Zhang, I. Romero-Canelón, A. Habtemariam, M. S. Cooper, L. Meszaros, G. J. Clarkson, P. J. Blower and P. J. Sadler (2017) In-cell activation of organo-osmium (II) anticancer complexes. *Angew. Chem. Int. Ed.* **56**, 1017–1020.
9. Zhang, X., F. Ponte, E. Borfecchia, A. Martini, C. Sanchez-Cano, E. Sicilia and P. J. Sadler (2019) Glutathione activation of an organometallic half-sandwich anticancer drug candidate by ligand attack. *Chem. Commun.* **55**, 14602–14605.
10. Zhang, W.-Y., S. Banerjee, G. M. Hughes, H. E. Bridgewater, J.-I. Song, B. Breeze, G. J. Clarkson, J. P. C. Coverdale, C. Sanchez-Cano, F. Ponte, E. Sicilia and P. J. Sadler (2020) Ligand-centred redox activation of inert organoiridium anticancer catalysts. *Chem. Sci.* **11**, 5466–5480.
11. Dougan, S. J., M. Melchart, A. Habtemariam, S. Parsons and P. J. Sadler (2006) Phenylazo-pyridine and phenylazo-pyrazole chlorido ruthenium(II) arene complexes: Arene loss, aquation and cancer cell cytotoxicity. *Inorg. Chem.* **45**, 10882–10894.

12. Mitra, K., S. Patil, P. Kondaiah and A. R. Chakravarty (2015) 2-(Phenylazo)pyridineplatinum(II) catecholates showing photocytotoxicity, nuclear uptake, and glutathione-triggered ligand release. *Inorg. Chem.* **54**, 253–264.
13. Dougan, S. J., A. Habtemariam, S. E. McHale, S. Parsons and P. J. Sadler (2008) Catalytic organometallic anticancer complexes. *Proc. Natl Acad. Sci. USA* **105**, 11628–11633.
14. Price, J. H., A. N. Williamson, R. F. Schramm and G. B. Wayland (1972) Palladium(II) and platinum(II) alkyl sulfoxide complexes. Examples of sulfur-bonded, mixed sulfur- and oxygen-bonded, and totally oxygen-bonded complexes. *Inorg. Chem.* **11**, 1280–1284.
15. Frisch, M. J., G. W. Trucks, H. B. Schlegel, G. E. Scuseria, M. A. Robb, J. R. Cheeseman, J. A. Jr Montgomery, T. Vreven, K. N. Kudin, J. C. Burant, J. M. Millam, S. S. Iyengar, J. Tomasi, V. Barone, B. Mennucci, M. Cossi, G. Scalmani, N. Rega, G. A. Petersson, H. Nakatsuji, M. Hada, M. Ehara, K. Toyota, R. Fukuda, J. Hasegawa, M. Ishida, T. Nakajima, Y. Honda, O. Kitao, H. Nakai, M. Klene, X. Li, J. E. Knox, H. P. Hratchian, J. B. Cross, V. Bakken, C. Adamo, J. Jaramillo, R. Gomperts, R. E. Stratmann, O. Yazyev, A. J. Austin, R. Cammi, C. Pomelli, J. W. Ochterski, P. Y. Ayala, K. Morokuma, G. A. Voth, P. Salvador, J. J. Dannenberg, V. G. Zakrzewski, S. Dapprich, A. D. Daniels, M. C. Strain, O. Farkas, D. K. Malick, A. D. Rabuck, K. Raghavachari, J. B. Foresman, J. V. Ortiz, Q. Cui, A. G. Baboul, S. Clifford, J. Cioslowski, B. B. Stefanov, G. Liu, A. Liashenko, P. Piskorz, I. Komaromi, R. L. Martin, D. J. Fox, T. Keith, M. A. Al-Laham, C. Y. Peng, A. Nanayakkara, M. Challacombe, P. M. W. Gill, B. Johnson, W. Chen, M. W. Wong, C. Gonzalez and J. A. Pople (2004) Gaussian 03, (Revision D 0.1), Gaussian Inc.
16. Perdew, J. P., K. Burke and M. Ernzerhof (1996) Generalized gradient approximation made simple. *Phys. Rev. Lett.* **77**, 3865–3868.
17. Hay, P. J. and W. R. Wadt (1985) Ab initio effective core potentials for molecular calculations. Potentials for the transition metal atoms Sc to Hg. *J. Chem. Phys.* **82**, 270–283.
18. McLean, A. D. and G. S. Chandler (1980) Contracted Gaussian basis sets for molecular calculations. I. Second row atoms, $Z$=11–18. *J. Chem. Phys.* **72**, 5639–5648.
19. Casida, M. E., C. Jamorski, K. C. Casida and D. R. Salahub (1998) Molecular excitation energies to high-lying bound states from time-dependent density-functional response theory: Characterization and correction of the time-dependent local density approximation ionization threshold. *J. Chem. Phys.* **108**, 4439–4449.
20. Cossi, M., N. Rega, G. Scalmani and V. Barone (2003) Energies, structures, and electronic properties of molecules in solution with the C-PCM solvation model. *J. Comput. Chem.* **24**, 669–681.
21. Browne, W. R., N. M. O'Boyle, J. J. McGarvey and J. G. Vos (2005) Elucidating excited state electronic structure and intercomponent interactions in multicomponent and supramolecular systems. *Chem. Soc. Rev.* **34**, 641–663.
22. O'Boyle, N. M. and J. G. Vos (2005) GaussSum, Dublin City University. Available at http://gausssum.sourceforge.net
23. Aird, R. E., J. Cummings, A. A. Ritchie, M. Muir, R. E. Morris, H. Chen, P. J. Sadler and D. I. Jodrell (2002) In vitro and in vivo activity and cross resistance profiles of novel ruthenium(II) organometallic arene complexes in human ovarian cancer. *Br. J. Cancer* **86**, 1652–1657.
24. Vichai, V. and K. Kirtikara (2006) Sulforhodamine B colorimetric assay for cytotoxicity screening. *Nat. Protoc.* **1**, 1112–1116.
25. Borenfreund, E. and J. A. Puerner (1985) Toxicity determined in vitro by morphological alterations and neutral red absorption. *Toxicol. Lett.* **24**, 119–124.
26. Traynor, N. J., P. E. Beattie, S. H. Ibbotson, H. Moseley, J. Ferguson and J. A. Woods (2005) Photogenotoxicity of hypericin in HaCaT keratinocytes: implications for St. John's Wort supplements and high dose UVA-1 therapy. *Toxicol. Lett.* **158**, 220–224.
27. Rauth, G. K., S. Pal, D. Das, S. Chittaranjan, A. M. Z. Slawin and J. D. Woollins (2001) Synthesis, spectral characterization and electrochemical studies of mixed-ligand complexes of platinum(II) with 2-(arylazo)pyridines and catechols. Single-crystal X-ray structure of dichloro{2-(phenylazo) pyridine}platinum(II). *Polyhedron* **20**, 363–372.
28. Panda, M., S. Das, G. Mostafa, A. Castiñeiras and S. Goswami (2005) Platinum complexes of diazoligands. Studies of regioselective aromatic ring amination, oxidative halogen addition and reductive halogen elimination reactions. *Dalton Trans.* 1249–1255.
29. Rochon, F. F., C. Bensimon and C. Tessier (2008) Multinuclear magnetic resonance study of Pt(II) compounds with sulfoxide ligands and crystal structures of complexes of the types $[Pt(R_2SO)X_3]^-$ and $Pt(R_2SO)_2Cl_2$. *Inorg. Chim. Acta* **361**, 16–28.
30. Muller, P., B. Schroder, J. Parkinson, N. Kratochwil, R. A. Coxall, A. Parkin, S. Parsons and P. J. Sadler (2003) Nucleotide cross-linking induced by photoreactions of platinum(IV)–azide complexes. *Angew. Chem. Int. Ed.* **42**, 335–339.
31. Wimmer, S., P. Castan, F. L. Wimmer and N. P. Johnson (1998) Aqueous chemistry of Pt(II) and Pd(II) complexes of 2,2′-bipyridine and 1,10-phenanthroline: pH dependence. *Inorg. Chim. Acta* **142**, 13–15.
32. Kamath, S. S., V. Uma and T. S. Srirastava (1989) Spectroscopic and electrochemical studies of some α-diimine complexes of platinum(II) and palladium(II) with azide and chloride. *Inorg. Chim. Acta* **161**, 49–56.
33. Anderson, R. G. and G. Nickless (1967) Metal complexes of some azo and azomethine dyestuffs: Part III. Metal complexes of 2-(2-pyridylazo)phenol and 4-(2-pyridylazo) phenol. *Anal. Chim. Acta* **39**, 469–477.
34. Ghedini, M., D. Pucci, A. Crispini and G. Barberio (1999) Oxidative addition to cyclometalated azobenzene platinum(II) complexes: a route to octahedral liquid crystalline materials. *Organometallics* **18**, 2116–2124.
35. Salassa, L., C. Garino, A. Albertino, G. Volpi, C. Nervi, R. Gobetto and K. I. Hardcastle (2008) Computational and spectroscopic studies of new rhenium(I) complexes containing pyridylimidazo[1,5-*a*]pyridine ligands: charge transfer and dual emission by fine-tuning of excited states. *Organometallics* **27**, 1427–1435.
36. Krause, R. A. and K. Krause (1980) Chemistry of bipyridyl-like ligands. Isomeric complexes of ruthenium(II) with 2-(phenylazo) pyridine. *Inorg. Chem.* **19**, 2600–2603.
37. Suppan, P. and N. M. Ghoneim (1997) *Solvatochromism*. Royal Society of Chemistry, Cambridge.
38. Lambert, J. B., H. F. Shurvell, D. A. Lightner and R. G. Cooks (1998) *Organic Structural Spectroscopy*. Prentice-Hall, New Jersey.
39. Garza-Ortiz, A., H. den Dulk, J. Brouwer, K. Jaap, S. Huub, A. L. Spek and J. Reedijk (2007) The synthesis, chemical and biological properties of dichlorido(azpy)gold(III) chloride (azpy = 2-(phenylazo)pyridine) and the gold-induced conversion of the azpy ligand to the chloride of the novel tricyclic pyrido[2,1-*c*][1,2,4]benzotriazin-11-ium cation. *J. Inorg. Biochem.* **101**, 1922–1930.
40. Garino, C. and L. Salassa (2013) The photochemistry of transition metal complexes using DFT. *Phil. Trans. R. Soc. A* **371**, 20120134.
41. Šima, J. (2006) Photochemistry of azide-moiety containing inorganic compounds. *Coord. Chem. Rev.* **250**, 2325–2334.
42. Ruggiero, E., S. Alonso-de Castro, A. Habtemariam and L. Salassa (2014) The photochemistry of transition metal complexes and its application in biology and medicine. In: *Luminescent and photoactive transition metal complexes as biomolecular probes and cellular reagents. Structure and Bonding*, Vol. **165** (edited by K. W. Lo), Springer, Berlin, Heidelberg.